Surfactant effects in model airway closure experiments

K. J. CASSIDY,[1] D. HALPERN,[2] B. G. RESSLER,[1] AND J. B. GROTBERG[3]
[1]*Department of Biomedical Engineering, Northwestern University, Evanston, Illinois 60208;*
[2]*Department of Mathematics, University of Alabama, Tuscaloosa, Alabama 35487; and*
[3]*Department of Biomedical Engineering, University of Michigan, Ann Arbor, Michigan 48109*

Cassidy, K. J., D. Halpern, B. G. Ressler, and J. B. Grotberg. Surfactant effects in model airway closure experiments. *J. Appl. Physiol.* 87(1): 415–427, 1999.—The capillary instability that occurs on an annular film lining a tube is studied as a model of airway closure. Small waves in the film can amplify and form a plug across the tube. This dynamical behavior is studied using theoretical models and bench-top experiments. Our model predicts the initial growth rate of the instability and its dependence on surfactant effects. In experiments, an annular film is formed by infusion of water into an initially oil-filled glass capillary tube. The thickness of the oil film varies with the infusion flow rate. The instability growth rate and closure time are measured for a range of film thicknesses. Our theory predicts that a thinner film and higher surfactant activity enhance stability; surfactant can decrease the growth rate to 25% of its surfactant-free value. In experiments, we find that surfactant can decrease the growth rate to 20% and increase the closure time by a factor of 3.8. Functional values of a critical film thickness for closure support the theory that it increases in the presence of surfactant.

pulmonary surfactants; surface tension; closing volume; airway liquid lining; microgravity

THE LUNG'S AIRWAYS are liquid-lined flexible tubes. It is well recognized that the liquid lining of the lung can close off a small airway by forming a liquid plug and/or by provoking the collapse of the flexible airway wall (17, 32). The formation of a plug blocks airflow and can further induce the complete collapse of an airway, since liquid continuously drains into the plug. This is a postclosure filling flow, which extends the axial length of the plug. This happens most frequently near the end of expiration, when the airway diameters are small, i.e., at the closing volume. During inhalation the airways expand, which may result in the rupture of the plug and the reestablishment of airflow to the periphery (13, 23, 34). The closure and subsequent reopening of these airways contribute to the shape of the pressure-volume curve in cycled lungs, which characterizes the mechanical response of the lung. Understanding the phenomena that determine it is a fundamental inquiry in pulmonary physiology in normal and microgravity environments. Measuring the occurrence of airway closure is one component of a standard pulmonary function test: the single-breath nitrogen-washout test. When this test shows early airway closure, it is often interpreted that there is inhomogeneous ventilation distribution within the lung, which may be caused by a number of normal and pathological conditions (6). Surfactants tend to stabilize the lining from closure, as has been shown qualitatively (31).

There are likely several contributing forces that lead to airway closure. Studies by Halpern and Grotberg (20, 21) have modeled closure, including the effects of a flexible wall. We focus on modeling closure of smaller airways, typically beyond and including *generation 16*, in which gravitational effects are small. Our present study investigates one of the key mechanisms believed to cause airway closure: a surface tension-driven instability. By isolating the experimental system from gravitational and flexible-wall effects, we are able to focus on the effects of the surface tension instability on closure and the relative effects of surfactant.

A capillary instability occurs on the wavy interface between two fluids. A circular-cylindrical tube is lined with a uniform layer (the film) of viscous fluid surrounding a less viscous fluid (the core). It is well known that this configuration is unstable to finite-wavelength disturbances. We use a rigid-tube experimental model and compare the experimental results with rigid-tube theory. Depending on the initial film thickness, such disturbances may culminate in stable, steady, finite-amplitude waves or lead to a topological transition in which the film completely pinches off the core fluid, forming a liquid plug. We examine the effects of surfactant on the surface tension-induced instability that contributes to airway closure.

Glossary

We find it helpful to convert some dimensional variables into dimensionless variables. We use the following guide to define which are dimensional and dimensionless. Greek symbols representing the fixed fluid parameters (μ and ρ) are dimensional, and changing fluid parameters are dimensionless unless indicated with an asterisk. Roman variables representing the fixed system parameters (a, b, and g) are dimensional, and all other Roman variables are dimensionless unless indicated with an asterisk.

a	Inner radius of the rigid tube
b	Radius of the undisturbed cylinder of fluid (core radius)
C^*	Bulk concentration of surfactant
Ca	$\mu_{film}U^*/\sigma^*$, capillary number for film formation
D_s^*	Surface diffusivity of surfactant
D	$\mu_{film}D_s^*/(h_0^*\sigma_m^*\bar{\delta})$
$\mathscr{D}$	$\epsilon^{-3}D$
$\bar{\delta}$	$-(\Gamma_m^*/\sigma_m^*)^{d\sigma^*}/_{d\Gamma^*\mid\Gamma^*=\Gamma_m^*}$, Marangoni number
$\hat{\delta}$	$\epsilon^{-2}\bar{\delta}$, surface activity parameter
ϵ	$(a - b)/a$, dimensionless thickness of the undisturbed film

The costs of publication of this article were defrayed in part by the payment of page charges. The article must therefore be hereby marked "*advertisement*" in accordance with 18 U.S.C. Section 1734 solely to indicate this fact.

ϵ_{crit}	Critical dimensionless film thickness
ϵ_f	Functional value of ϵ_{crit} (taken at $t_c = 2 \times 10^4$)
g	Gravitational constant
Γ^*	Surface concentration of surfactant
Γ^*_m	Mean surface concentration of surfactant
Γ	$\Gamma^*/\Gamma^*_m = 1 + \epsilon^2\overline{\Gamma}$
$\overline{\Gamma}$	Variation of surface concentration from the mean
$\hat{\Gamma}$	$\epsilon^2\overline{\Gamma}$
h^*_0	Undisturbed film thickness
h^*	Amplitude of the film disturbance
h	$h^*/\epsilon a$
h_1	Initial amplitude (perturbation parameter)
k^*	$2\pi/\lambda^*$, wave number of the disturbance
k	k^*a
K	k^*b
k^*_1	Surfactant adsorption constant
k^*_2	Surfactant desorption constant
λ^*	Wavelength of the disturbance
λ	λ^*/a
μ_{core}	Viscosity of the core fluid
μ_{film}	Viscosity of the film fluid
q^*	Initial growth rate of the disturbance
q	$q^*a\mu_{film}/\sigma^*$
$\hat{q}$	$q^*\epsilon^{-3}a\mu_{film}/\sigma^*$
r	r^*/a, radial distance from the tube axis
ρ_{core}	Density of the core fluid
ρ_{film}	Density of the film fluid
σ^*	Surface tension at the interface between the fluids
σ^*_m	Mean value of surface tension
t^*_f	Final time of the disturbance (at closure)
t^*_0	Start time of the disturbance
t^*_c	$t^*_f - t^*_0$, total time for closure to occur
t	$t^*/(a\mu_{film}/\sigma^*)$
$\hat{t}$	$t^*/(\epsilon^{-3}a\mu_{film}/\sigma^*)$
U^*	Mean velocity of the infused core fluid (during film formation)
z	z^*/a, distance along the tube axis

PREVIOUS RESEARCH

Mechanical phenomena related to airway closure can be drawn from several sources. From the physiological literature, the stabilizing effects of surfactants on models of airway closure have been demonstrated. Liu et al. (31) conducted experiments where air is forced through a narrow glass or esophageal tube segment initially filled with saline or a surfactant-saline solution. They used a constant tube size and driving pressure, with a constant liquid volume localized to the narrow, constricted segment of the tube. The liquid in the tube gives way to airflow but reforms a plug in systems with little surfactant or surfactant weakened by albumin and fibrinogen. However, the plug does not reform if adequate surfactant is present, for the conditions explored. This demonstrates the important clinical effects of exogenous surfactant replacement therapy (11, 30, 44), which can help stabilize airways in patients who have a surfactant deficiency. Liu et al. attributed this additional stability to the reduction of surface tension caused by the surfactant polar molecules. Saline lung lavage in isolated rat lungs reduces the endogenous surfactant concentration, causing an increase in airway resistance due to rapid plug formation (7, 8). However, instillation of exogenous calf lung surfactant extract after the lavage can increase the duration of unobstructed airway time by a factor of 3 (8) to 7 (7), determined by measuring resistance via airway pressure. It would be interesting to examine the airway closure and film amplification for a range of initial film thicknesses and compare behavior before and after addition of exogenous surfactant.

From the engineering literature, the study of capillary instabilities, such as the breakup of a cylindrical column of fluid or a thin film coating a rigid tube, continues to be an area of ongoing investigation. Plateau (37) considered the static stability of a cylindrical column of fluid with undisturbed radius b. He proved, using energy arguments, that a perturbation to the interface is unstable if its wavelength (λ^*) exceeds the circumference of the column ($2\pi b$). The perturbation causes axial waves in the interface, similar to waves in the interface of our system, which we show and discuss in *Experimental methods*. Rayleigh (40) studied the dynamic stability of an initially cylindrical liquid jet. He found that waves at the surface amplify until the jet breaks up into a stream of droplets, provided Plateau's criterion holds, i.e., that $K < 1$, where $K = k^*b = 2\pi/\lambda^*$ is the disturbance wave number. Rayleigh derived a relationship between the disturbance growth rate (q^*) and K. The q^* attains a maximum at some critical wave number (K_{crit}). He found the least-stable mode at $K_{crit} = \pi/4.5 \approx 0.698$ for a liquid jet in an inviscid or a viscous fluid. Rayleigh (41) modified this analysis for a jet of air immersed in a liquid and found the same criterion for the maximum growth rate (q_{max}): $K_{crit} = \pi/4.5$.

Goren (16) studied the stability of an annular liquid film lining a tube otherwise filled with air. A rigid tube of radius a, lined with a uniform film at radial distance b, has a dimensionless film thickness $\epsilon = (a - b)/a$. A disturbance of λ^* causes axial waves in the interface, which can amplify and eventually cause film closure. Goren performed experiments for $0.06 < \epsilon < 0.33$ and allowed the systems to reach closure. Plug formation occurred at multiple, spatially periodic locations defined by K_{crit}, which was shown to depend weakly on ϵ. In his accompanying theoretical analysis for the initial growth rate, $q = q^*a\mu_{film}/\sigma^*$, (where μ_{film} is viscosity of the fluid film), he predicts how q_{max} depends on K_{crit} and ϵ. Goldsmith and Mason (15) performed closure experiments using immiscible liquids of similar density for the film and core fluids to minimize buoyancy. They measured disturbance wave numbers that match Goren's theory well and initial growth rates that were slightly greater than predicted by theory (16). Sample results are shown tracing the logarithm of the amplitude of the growth vs. time for two experiments, at $\epsilon = 0.19$ and $\epsilon = 0.25$, on a surfactant-free system. The disturbance amplitude initially grows exponentially with time, at a constant q, but as the wave amplifies, q

accelerates. Also, the closure times (t_c) of the two sample experiments can be depicted from this graph.

The ϵ must be larger than a critical value (ϵ_{crit}) for closure to occur. Disturbance waves in a film that is thinner than ϵ_{crit} may amplify to form undulate collars spaced throughout the tube. However, not enough liquid volume is present for the collars to bridge the tube. Everett and Haynes (9) found that a collar of surfactant-free fluid wetting a rigid tube would undergo a topological transformation to a liquid plug, provided the collar volume exceeds $5.47a^3$ enclosed within one axial wavelength. Similar results were also obtained by Kamm and Schroter (28), who conducted experiments where oil is dripped into small vertical rigid tubes. By assuming an initial film thickness of 10 μm at total lung capacity (TLC), they estimated that airway closure first occurs in the terminal bronchioles (about *generations 16–17*) at a lung volume of 23% TLC. For an initial film thickness of 5 μm, airway closure first occurs at 12% TLC (28). These closing volumes are commonly seen in pulmonary function tests.

Gauglitz and Radke (12), extending theoretical work by Hammond (22), computed an $\epsilon_{crit} = 0.12$ necessary for closure, whereas their experiments indicate an average $\epsilon_{crit} = 0.09$. Johnson et al. (27) analyzed the stability of a viscous annular film, including the effects of inertia. They found their approximation of the initial growth rate to match Goren's exact solution well. Closure of liquid-lined, linearly elastic tubes has been investigated by Halpern and Grotberg (20). They found that flexibility enhances the growth of the unstable film. Theoretical models developed to examine the effects of surfactant on film stability (21, 35) show that plug formation in a system containing surfactant is slowed by a factor of ~4 over the surfactant-free model. Halpern and Grotberg (21) found that ϵ_{crit} is increased in a system containing surfactant, and ϵ_{crit} decreases with increasing ratio of surface forces to elastic forces.

In EXPERIMENTS, we describe the materials and methods for performing experiments on annular film closure in a capillary tube. We consider a range of initial film thicknesses and examine systems without and with surfactant. The experimental system uses liquids for the core and film fluids that approximately match the viscosity ratio and Reynolds numbers (Re) in the lung system. Gravitational effects are negligible, inasmuch as the density difference between the core and film liquids is small. This allows us to investigate the closure phenomena induced by nongravitational forces. Also, film closure occurs much more slowly in a liquid-liquid system than in an air-liquid system, allowing the film dynamics to be viewed and recorded in real time. Then we report the experimental results of t_c, q, and ϵ_{crit}; we also report inflow results of the annular film formation. Next we outline our theoretical model for the initial growth rate in a system containing surfactant and show theoretical results. Then we discuss some observed behavior, compare the experimental data with theory, and make conclusions about the effects of surfactant on film formation and stability.

EXPERIMENTS

Materials. Four fluid systems are used in these sets of experiments (Table 1). We use high-viscosity oils as the film fluid and water as the core fluid. In *systems 1* and *2*, the oil used for the annular film is LB-1715 (Union Carbide Chemical, South Charleston, WV), which is a propylene glycol monobutyl ether. *System 1* is surfactant free, and *system 2* contains a small amount of the surfactant 1-palmitoyl-2-lauroyl-*sn*-glycero-3-phosphocholine (Avanti Polar Lipids, Alabaster, AL; PLPC). It is an asymmetric fatty acid that is insoluble in water. *System 2* contains 10^{-3} mM bulk concentration of PLPC dissolved in the oil phase before contact with the water phase. In *systems 3* and *4*, the oil used for the annular film is LB-400-X (Union Carbide Chemical). *System 3* is surfactant free, and *system 4* contains a small amount of the surfactant Tween 20 (Sigma Chemical, St. Louis, MO). Tween 20 is polyoxyethylenesorbitan monolaurate and is made up of various fatty acids; it is soluble in water and insoluble in oil. It is initially dissolved in the water phase at a bulk concentration of 0.01% by weight. In Table 1 the film viscosities were measured at room temperature (24–25°C) with an Oswald bulb viscometer, and the film densities are from manufacturer specifications. The surface tension of the LB-1715 and LB-400-X in air is 33–38 dyn/cm. Mean values for the surface tension of an oil-water interface were measured using a ring tensiometer and are displayed in Table 1. In calculations that require a value for the surface tension (σ^*) for these experiments, we use the mean values for each of the four systems.

Similitude: matching parameters. The system parameters are organized into dimensionless groups (Table 2). We attempt to model the ranges found in the pulmonary airways, with some important differences. We assume that at *generation 16* in normal lungs the film is the aqueous phase with a mean airway diameter of 0.049 cm (46). In calculating lung properties in Table 2, we use the density and viscosity values of water and air for the film and core fluids, respectively. The surface tension varies by region of the lung because of the local quantity of surfactant and by lung volume because of dynamic surface concentration of surfactant. The tracheal surface tension was directly measured to be 31 dyn/cm in normal horse lungs (24) and 33 and 32 dyn/cm in normal rat and guinea pig lungs, respectively (29). The equilibrium surface tension in the alveolar region of rabbit lungs was

Table 1. *Properties of the experimental systems*

System No.	Film Fluid	Core Fluid	Surfactant	Concentration	σ^*, dyn/cm	μ_{film}, cStokes	ρ_{film}, g/cm^3
1	LB-1715	Water	None	0	4.59	770	0.997
2	LB-1715	Water	PLPC	10^{-3} mM	4.23	770	0.997
3	LB-400-X	Water	None	0	4.77	150	0.989
4	LB-400-X	Water	Tween 20	0.01% (by wt)	2.88	150	0.989

PLPC, 1-palmitoyl-2-lauroyl-*sn*-glycero-3-phosphocholine; σ^*, surface tension at interface between fluids; μ_{film}, viscosity of film fluid; ρ_{film}, density of film fluid.

Table 2. *Dimensionless parameters for the pulmonary system and the experimental models*

Dimensionless Parameter	Description	Normal Lung (at *generation 16*)	Experiments
$\epsilon = \frac{(a-b)}{a}$	Undisturbed film thickness	0.02–0.04	0.12–0.36
$\epsilon^{-1}\mathrm{Bo} = \frac{\Delta\rho g a^2}{\sigma^* \epsilon}$	Effective Bond number	0.3 (for $\epsilon = 0.15$)	10^{-3}–3×10^{-2}
$\gamma = \frac{\mu_{core}}{\mu_{film}}$	Viscosity ratio	10^{-2}	10^{-3}–7×10^{-2}
$\epsilon^2\,\mathrm{Re}_{film} = \frac{\epsilon^5\rho_{film}\sigma^* a}{\mu_{film}^2}$	Effective Reynolds number for film fluid	10^{-6}–10^{-3}	10^{-8}–10^{-4}
$\epsilon^2\,\mathrm{Re}_{core} = \frac{\epsilon^5\rho\sigma^* a}{\mu_{film}\mu_{core}}$	Effective Reynolds number for core fluid	10^{-9}–10^{-4}	10^{-5}–5×10^{-2}
$\beta = \frac{k_1^* C^*}{k_2^* h_0^*}$	Solubility parameter	10^6–10^7	10^6
$\mathscr{D} = \epsilon^{-3}\mathrm{D} = \frac{\mu_{film} D_s^*}{\epsilon^3 h_0^* \sigma_m^* \bar{\delta}}$	Surface diffusivity	10^{-3}–10^{-1}	10^{-4}–10^{-2}

measured to be 7 and 30 dyn/cm at 50 and 100% TLC, respectively (43). We expect the surface tension in normal pulmonary airways to be ~20–25 dyn/cm at functional residual capacity, which agrees with previously published values (14, 18). We use $\sigma^* = 20$ dyn/cm in Table 2 for calculations of normal lung parameters at *generation 16*.

In normal lungs the film lining is very thin, but many diseases as well as the state of lung inflation can affect ϵ, the ratio of film lining thickness to airway radius. Yager et al. (48) measured the airway surface liquid thickness in the small airways of the guinea pig. With use of data from their Fig. 4 on the airway perimeter and film thickness, and the assumption that the airways are approximately circular in cross section, the average ratio of film thickness to airway radius is 0.02. In a study by Codd et al. (4), in a sheep trachea, the mean $\epsilon = 0.04$. Excessive bronchial secretions in individuals with unhealthy lungs can commonly produce airway surface liquid films that are 10% of the airway diameter (42); this corresponds to $\epsilon = 0.20$. In our experiments we model airways in which the film is thick enough to close: $\epsilon > 0.12$.

The Bond number (Bo) = $\Delta\rho g\, a^2/\sigma^*$ (where ρ is fluid density and g is gravitational constant) indicates where gravitational effects are significant. Here, $\Delta\rho = |\rho_{film} - \rho_{core}|$, the difference in densities between the two fluids. Gravity can be neglected, provided ϵ^{-1} Bo $\ll 1$ (22), which generally holds in smaller airways. Under normal-gravity conditions, for $\epsilon = 0.15$, we calculate that ϵ^{-1} Bo < 0.3, starting at *generation 16* in adults and starting at *generation 9* in infants. In the case of lessened gravity (such as the microgravity environment) or higher surface tension (which can occur in premature infants born with insufficient pulmonary surfactant) the Bo values would be smaller. In our experiments we wish to examine the dynamics of closure as contributed by forces other than gravitational. By using a liquid-liquid system, where the fluid densities are similar, we can create systems with low Bo values by reducing $\Delta\rho$. The time scale of these experimental systems is larger than the air-liquid system in the airways by a factor of 10^4. By slowing the closure process, data capture is simplified, with improved accuracy in the results. These fluids are chosen, oil for the film and water for the core fluid, such that the viscosity ratio $\gamma = \mu_{core}/\mu_{film} \ll 1$, which matches the lungs. Fluid inertia is negligible, provided $\epsilon^2\,\mathrm{Re}_{film} = (\epsilon^5\rho_{film}\sigma^* a)/\mu_{film}^2 \ll 1$ (22), which is true in the lungs (Table 2). Similarly, fluid inertia in the core is neglected, since $\epsilon^2\,\mathrm{Re}_{core} = [(\epsilon^5\sigma^*)/\mu_{film}][(\rho_{core} a)/\mu_{core}] \ll 1$, as in the lungs.

To create a surfactant monolayer between the two fluid layers, we first dissolve the surfactant into one of the bulk fluids. When the interface between the two fluids is formed, we assume that the surfactant rapidly adsorbs to the surface and does not rapidly desorb back into the bulk of the fluid. By calculating the solubility parameter $\beta = (k_1^* C^*)/(k_2^* h_0^*)$, we can estimate the ratio of time scales for desorption to adsorption (26), where k_1^* is the adsorption coefficient, k_2^* is the desorption coefficient, C* is the bulk concentration of surfactant, and h_0^* is the film thickness. Jensen and Grotberg (26) estimate that the pulmonary surfactant component dipalmitoylphosphatidylcholine (DPPC) dissolved in an aqueous lung surface layer 1 μm thick will have $\beta = 5 \times 10^7$. At *generation 16* the airway surface liquid is ~6–12 μm thick (using $0.02 \le \epsilon \le 0.03$), yielding $4.2 \times 10^6 \le \beta \le 8.5 \times 10^6$. The surfactant PLPC used in our experiments has adsorptive/desorptive properties similar to DPPC. Using the range of film thicknesses found in our experiments (3.5 μm $\le h_0^* \le$ 10.4 μm), we estimate $1.4 \times 10^6 \le \beta \le 4.8 \times 10^6$ for the system containing PLPC. Because $\beta \gg 1$ in the lung and in our experiments, we assume that surfactant concentration at the interface is initially uniform. Surface diffusivity of surfactant is measured by the diffusivity parameter $\mathscr{D} = \epsilon^{-3}\mathrm{D}$, where $\mathrm{D} = -[(\mu_{film} D_s^*)/(h_0^* \sigma_m^* \bar{\delta})]$ and D_s^* is the dimensional surface diffusivity. The Marangoni number, defined as $\bar{\delta} = -(\Gamma_m^*/\sigma_m^*)^{d\sigma^*/d\Gamma^*|\Gamma^*=\Gamma^*_m}$, is a measure of the ability of the surfactant to lower the surface tension of a monolayer. Here, Γ_m^* is the mean value of Γ^*, the surface concentration of surfactant, and σ_m^* is the mean value of σ^*. Agrawal and Neuman (1) directly measured the surface diffusivity of DPPC in myristic acid and found $10^{-7} < D_s^* < 7 \times 10^{-5}$ cm^2/s. Jensen and Grotberg (25) approximate that D is on the order of 10^{-6} for experiments and 10^{-4} in an airway. For $\epsilon = 0.1$, this still makes $\mathscr{D}$ quite small: $10^{-3} \le \mathscr{D} \le 10^{-1}$. Therefore, the current theory neglects surface diffusivity.

Experimental methods. A thin cylindrical borosilicate glass capillary tube with an inner diameter of 0.058 cm and length of 20 mm is viewed under a microscope-camera configuration (Fig. 1). The glass capillary is cleaned with chromic acid, rinsed with acetone and deionized water, and dried before the

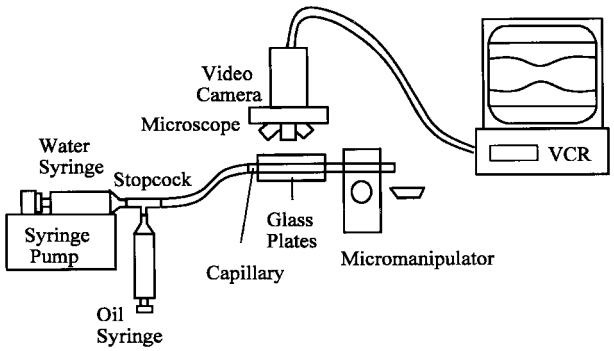

Fig. 1. Schematic of experimental apparatus.

experiment. Fluids are delivered to the capillary tube through flexible Teflon tubing having the same inner and outer diameters as the rigid capillary tube and held together by a sleeve of silicone tubing and glue. A three-way stopcock is used to direct the fluids from respective syringes through the Teflon tubing. The film fluid is injected manually, and a positive-displacement syringe pump (model 341-A, Sage Instruments) drives the core fluid through the tube. The capillary tube, immersed in glycerol and held between two glass slides perpendicular to the microscope to correct for visual distorsion, is then placed under the microscope and into a pipette holder, which is attached to a Leitz micromanipulator. A camera is attached to the top of a Leitz Laborlux D microscope; the capillary tube is viewed at ×200 or ×500 magnification. All experiments are recorded from a Javelin JE3362 camera connected to a JVC SR-S360 video recorder. A Sony PVM-2030 20-in. color monitor is also connected, which provides for viewing capabilities during experiments and later for data acquisition.

To measure the value of the mean interfacial surface tension between the film fluid and the core fluid, we use a standard 6-cm platinum-iridium ring tensiometer. Measuring accurately the surface tension between liquids of similar densities can be difficult. In the tensiometer test, a thin ring is pulled up through the horizontal liquid-liquid interface, creating a vertical force on the ring, which is then measured by the tensiometer scale. However, a ring pulled through liquids of similar density may not produce a vertical interface, particularly on the inner edge of the ring. The inaccuracy may be quite large, since the ring tensiometer measures only the vertical component of the force. For contact angles deviating from vertical by up to 30°, the true surface tension may be underestimated by as much as 15%. Assuming a vertical interface, we estimate the mean surface tension of LB-1715 with deionized distilled water to be 4.59 dyn/cm. The addition of the surfactant PLPC added to the oil phase in molar bulk concentrations of 10^{-4}–10^{-1} mM causes a slight decrease in the mean surface tension to 4.23 dyn/cm (<8% change). The mean surface tension of LB-400-X and water, estimated at 4.77 dyn/cm, exhibits a dramatic decrease with the addition of 0.01% (by weight) Tween 20, to 2.88 dyn/cm (~40%).

As part of the preliminary steps in performing stability experiments, it is necessary to create the two-phase system of an annular film lining a tube with a fluid core. This system is established by first filling the tube with the film fluid from a 10-ml syringe. The core fluid is then pumped into the center of the tube, driven by a positive-displacement syringe pump. This core fluid flows through the center of the tube like a long finger (Fig. 2*A*) and leaves an axisymmetric annular film on the tube walls (Fig. 2*B*). The thickness of the film depends on the capillary number ($Ca = \mu_{film} U^*/\sigma^*$, where μ_{film} is the film viscosity, U^* is the average core fluid velocity, and σ^* is the interfacial surface tension). Previous studies (10, 15, 45) support an empirical equation for ϵ

$$\epsilon = 0.5Ca^{1/2} \quad (1)$$

for $10^{-4} < Ca < 10^{-1}$. Results from several experimental studies support Bretherton's theoretical analysis (2), indicating

$$\epsilon = 0.643(3Ca)^{2/3} \quad (2)$$

for $10^{-4} < Ca < 10^{-2}$. Martinez and Udell (33) conducted a numerical analysis on a finite-length bubble to describe the shape at the leading and trailing menisci. Their predictions of $\epsilon(Ca)$ are in excellent agreement with experimental data by Taylor (45) for $10^{-2} \leq Ca \leq 2$ and support *Eq. 1* for $10^{-2} \leq Ca \leq 10^{-1}$. Goldsmith and Mason (15) also performed experiments on two sets of fluid systems with and without the surfactant Tween 20. Without surfactant, they concluded that ϵ varies like $Ca^{0.5}$ for small Ca. However, when 0.5% Tween 20 is added to the water phase of the two systems, they find that ϵ varies like $Ca^{0.28}$ and $Ca^{0.44}$, respectively.

The average core fluid velocity is defined as the infusion flow rate divided by the measured cross-sectional area of the core. Using this relationship, we can directly control the formed film thickness by varying the flow rate settings on the syringe pump. In creating the annular film, syringe pump settings range from 0.35 ml/h to 0.49 ml/min. Here, films are

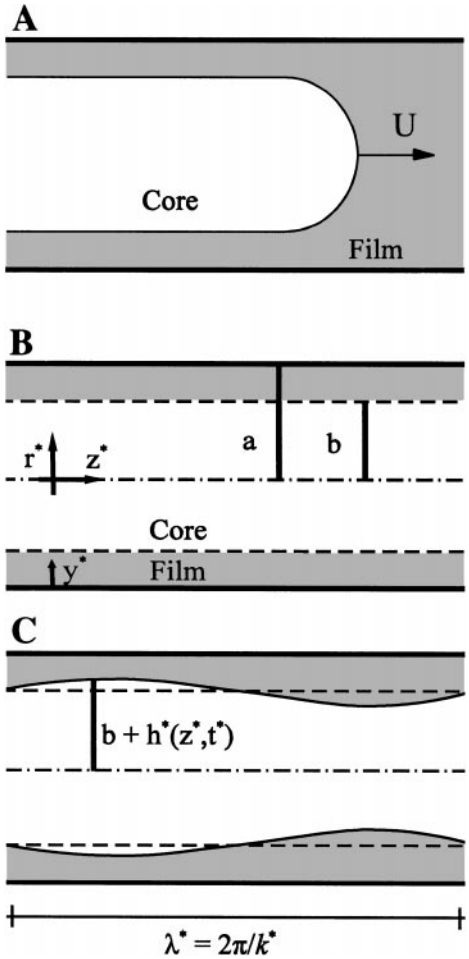

Fig. 2. Schematic of inflow (*A*), uniform annular film (*B*), and disturbed film (*C*). See *Glossary* for definition of abbreviations.

formed with $\epsilon \sim 0.12-0.36$. It is necessary to record ϵ before waves develop. Measurements of ϵ are taken at several locations between about two and five tube diameters from the leading meniscus of the infused core fluid, then averaged. Once the uniform film is established throughout the tube, the inflow is stopped and the downstream end of the tube is plugged. The tube is then scanned to search for small waves at the interface with use of a finely controlled micromanipulator, and wave amplification (Fig. 2*C*) is viewed and recorded.

Figure 3 shows six photographs taken from a sample experiment in its entirety; Fig. 3, *A* and *B*, are from the inflow part; Fig. 3, *C–F*, correspond to the film instability. We use Targa-Plus software and Frame-Grabber PC board. In Fig. 3*A* the film fluid is displaced by a finger of the core fluid, which leaves a uniform annular film, as shown in Fig. 3*B*. The infusion flow is shut off, then a small disturbance is located (Fig. 3*C*), which then amplifies (Fig. 3*D*). Measurements of the film interface evolution are taken at the longitudinal position where the radius of the interface is the smallest. Interface positions are recorded periodically, and the time at closure is noted. We see the film as it amplifies just before closure in Fig. 3*E*, then just after closure in Fig. 3*F*. The recorded data are analyzed to determine the initial, constant growth rates and the closure times as a function of ϵ and system parameters. For this sample experiment shown on *system 2*, recorded values are as follows: inflow rate = 2.7 ml/h, $\epsilon = 0.29$, $q^* = 0.155\ s^{-1}$, and closure time (t_c^*) = 24 s.

Determining t_c^* and initial growth rate. To extract t_c^* from an experimental trial, it is necessary to determine the start time (t_0^*) of the disturbance. However, a wave has already begun to amplify ($t^* > t_0^*$) before it is large enough to be visually detected. Below, we describe a method that allows the dimensional values of t_0^* and the initial growth rate q^* to be estimated. A small wave disturbance initially grows exponentially with time. A normal mode expression for $h = h_1 e^{q^* t^* + ik^* z^*}$ is used where $h = h^*/\epsilon a$ is a sinusoidal film amplitude. By plotting $\ln(h)$ vs. t^* from our data, the abscissa represents an arbitrary time corresponding to the time of the videotape recording. A straight-line curve fit to the early data results in the $t^* = 0$ intercept at $h = h_1$. The t_0^* of the perturbation is taken to be the time at which the disturbance amplitude is 5% of the undisturbed film thickness. The slope of the initial portion of this graph also gives q^* (in s^{-1}). Then $t_c^* = t_f^* - t_0^*$, where t_f^* is the final time documented at closure (in s). Values for the dimensionless growth rate and closure time are then computed.

EXPERIMENTAL RESULTS

In Figs. 4–6, involving our experimental data, symbols represent average values for a set of experiments. A "set" constitutes a group of film systems that were created by using a specific inflow rate to provide consistent values of ϵ for the set. There is some deviation within a set for ϵ, as well as the values of t_c [$t_c^*/(a\mu_{film}/\sigma^*)$], q [$q^* a\mu_{film}/\sigma^*$], and Ca. For this reason, bidirectional scatter bars, which are based on the standard deviation of the set, are shown. We used 13 flow settings in the range 0.35 ml/h to 0.49 ml/min. For each set, up to 20 experimental trials were performed and averaged. For the experiments on stability, useful data were extracted from two to eight trials per set. For inflow experiments establishing the uniform film thickness, the number of trials providing useful data varied from 2 to 20 per set.

Closure time and minimum film thickness. Figure 4 indicates how t_c decreases as ϵ increases and how the presence of surfactant delays closure. In Fig. 4*A*, the addition of PLPC to this system increases t_c by up to a factor of 3.8 (the value at $\epsilon = 0.19$). Note that for increasingly thick films, the difference between the surfactant-free and the surfactant data becomes less significant. In Fig. 4*B*, the addition of Tween 20 causes an increase in t_c by up to a factor of 3.0 (at $\epsilon = 0.24$). The thinnest films we found to close were at $\epsilon = 0.123$ for *system 1*, at $\epsilon = 0.154$ for *system 2*, at $\epsilon = 0.143$ for *system 3*, and at $\epsilon = 0.156$ for *system 4*.

The solid lines in Fig. 4 are computed from the surfactant-free theory of Halpern and Grotberg (20) in the rigid-tube limit. The dashed lines are computed from the theory of Halpern and Grotberg (21) that predicts closure in a system containing surfactant. We simultaneously solve their *Eq. A1* numerically. Values are chosen for the surface activity ($\bar{\delta} = 8$) and for the disturbance wavelength ($\lambda = 2^{3/2}\pi$) corresponding to a system with normal surface activity and a disturbance with the most dangerous wavelength. We calculated $\epsilon_{crit} = 0.13$ for a surfactant system using these values (20).

Initial growth rate of the disturbance. The q of the capillary instability is found to increase as ϵ increases and to decrease in the presence of surfactant. In Fig. 5*A*, the presence of PLPC in *system 2* decreases the growth rate to as little as 21% (at $\epsilon = 0.19$) of surfactant-free *system 1* values. In Fig. 5*B*, Tween 20 causes q to decrease to as little as 24% (at $\epsilon = 0.20$) of the corresponding surfactant-free values for these experiments.

In Fig. 5, the solid lines are a reproduction of Goren's theory (16) for the maximum growth rate (q_{max}) of a surfactant-free system of arbitrary thickness ϵ. We have calculated the theory line by rescaling the wave number on the tube radius, or $k = k^* a$. The three broken lines are from our linear theory of q_{max}, which is valid for thin films; we have shown lines representing the theory up to $\epsilon = 0.20$. The short-dashed line is our current theory in the limit of no surfactant, or $\bar{\delta} = 0$. Derivation of our present theory is detailed in LINEAR STABILITY ANALYSIS FOR THE AIRWAY CLOSURE MODEL WITH SURFACTANT. Details on the theoretical results follow the derivation in THEORETICAL RESULTS. The long-dashed and long-and-short-dashed lines show our theory for an interface with a small amount of surfactant ($\bar{\delta} = 0.01$) and saturated with surfactant ($\bar{\delta} = \infty$), respectively. Normal surface activity $\bar{\delta} = 8$ lies in the narrow margin between the very small and very large surfactant activity values. As the surface activity increases, the growth rate decreases. Note how even a small amount of surfactant can cause a significant decrease in the growth rate compared with the same system without surfactant.

Thickness of the annular film. The ϵ of the formed annular film is shown to increase with Ca for the inflow procedure in Fig. 6. In Fig. 6*A*, some experimental results of Goldsmith and Mason's surfactant-free *system 6a* (15) are also shown for comparison. There is a smooth transition between their data and ours. We find

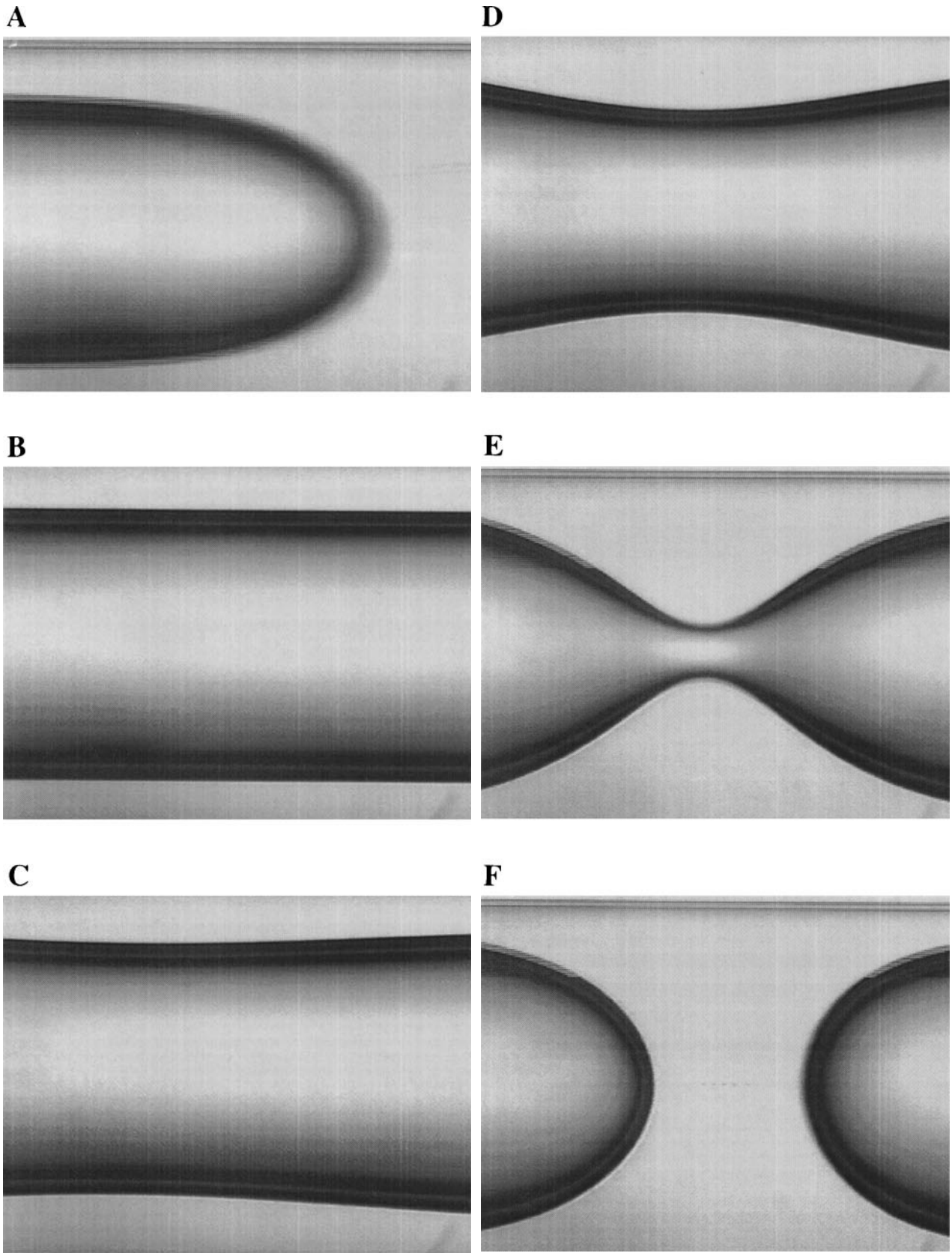

Fig. 3. Photographs of experimental procedure. Inflow begins (*A*) and a uniform film is established (*B*); then inflow is stopped, a small disturbance is located (*C*), and disturbance amplifies (*D*). *E*: just before closure. *F*: just after closure.

the asymptotic behavior as predicted by others (5, 33), with our experimental value near $\epsilon = 0.34$ at Ca = 10. In Fig. 6*B*, at a given Ca, ϵ decreases slightly in the presence of Tween 20, from *system 3* to *system 4*. However, the change in ϵ with the addition of surfactant is comparable to the experimental scatter, which is <10%. The long-dashed line is *Eq. 2*, Bretherton's theory (2), and the short-dashed line is *Eq. 1*, from Fairbrother and Stubbs (10). *Equation 2* is inaccurate for $Ca > 10^{-2}$ and overpredicts ϵ for all our experiments in this study. *Equation 1* matches ϵ well for $Ca < 0.2$ but is invalid for large Ca and overpredicts ϵ for $Ca > 0.2$. We reproduce the numerical results of Martinez and Udell (33) (solid line) for a surfactant-free system, in the range $10^{-2} < Ca < 10$. There is little variation in ϵ between *systems 1* and *2*, the deviation being comparable in size to the experimental scatter, which ranges from 2 to 13%.

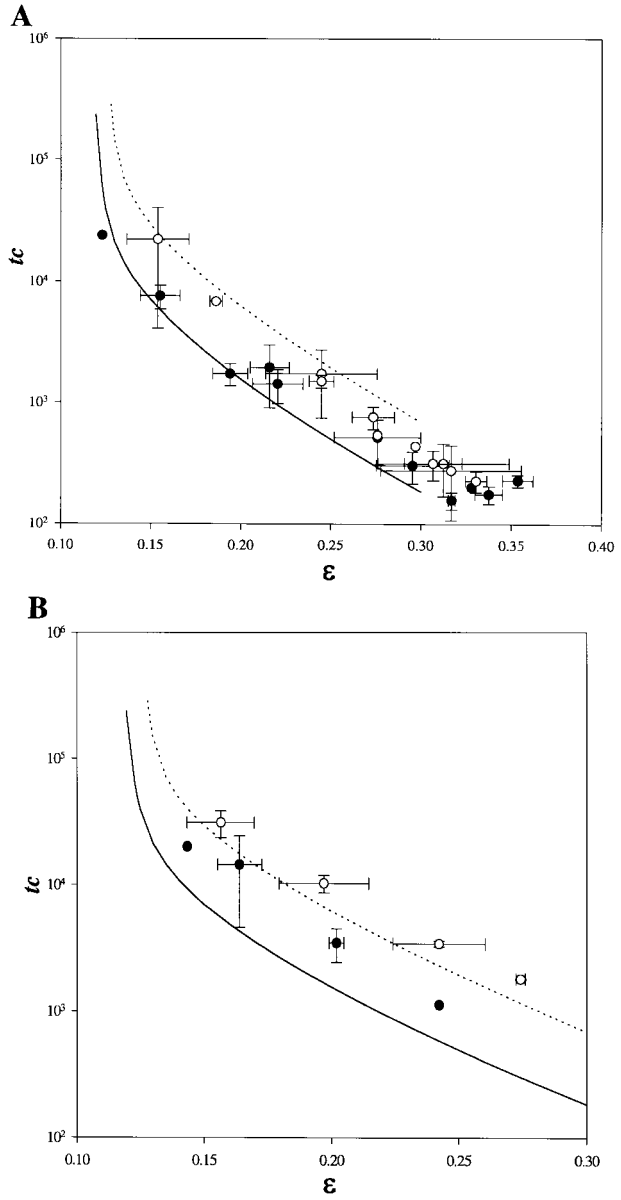

Fig. 4. Closure time [$t_c = t_c^*/(a\mu_{film}/\sigma^*)$] vs. undisturbed film thickness (ϵ) for *systems 1* (●) and *2* (○; *A*) and *systems 3* (●) and *4* (○; *B*). Surfactant delays closure, and thicker films take longer to close than thinner films. Note how closure time tends to infinity as ϵ approaches ϵ_{crit}. See text for theoretical curves.

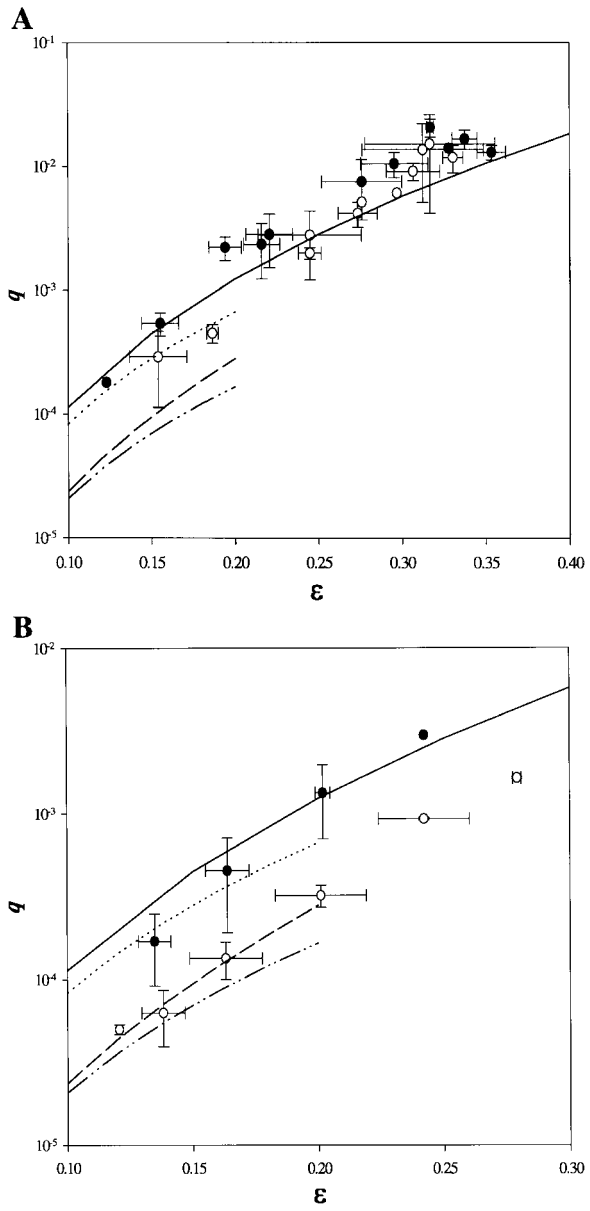

Fig. 5. Initial growth rate ($q = q^*a\mu_{film}/\sigma^*$) vs. ϵ for *systems 1* (●) and *2* (○; *A*) and *systems 3* (●) and *4* (○; *B*). Surfactant decreases growth rate, and thicker films grow faster than thinner films. See text for theoretical curves.

LINEAR STABILITY ANALYSIS FOR THE AIRWAY CLOSURE MODEL WITH SURFACTANT

A linear stability analysis is performed on the airway closure model with surfactant. The model is based on the inertia-free analysis developed by Halpern and Grotberg (20), who derived a system of nonlinear evolution equations (*Eq. A1*) for the film thickness and surface concentration of surfactant (see APPENDIX). To investigate linear stability of the system, we use normal-mode sinusoidal disturbances

$$h = h_1 e^{\hat{q}\hat{t} + ikz} \quad \text{and} \quad \hat{\Gamma} = \hat{\Gamma}_1 e^{\hat{q}\hat{t} + ikz} \qquad (3)$$

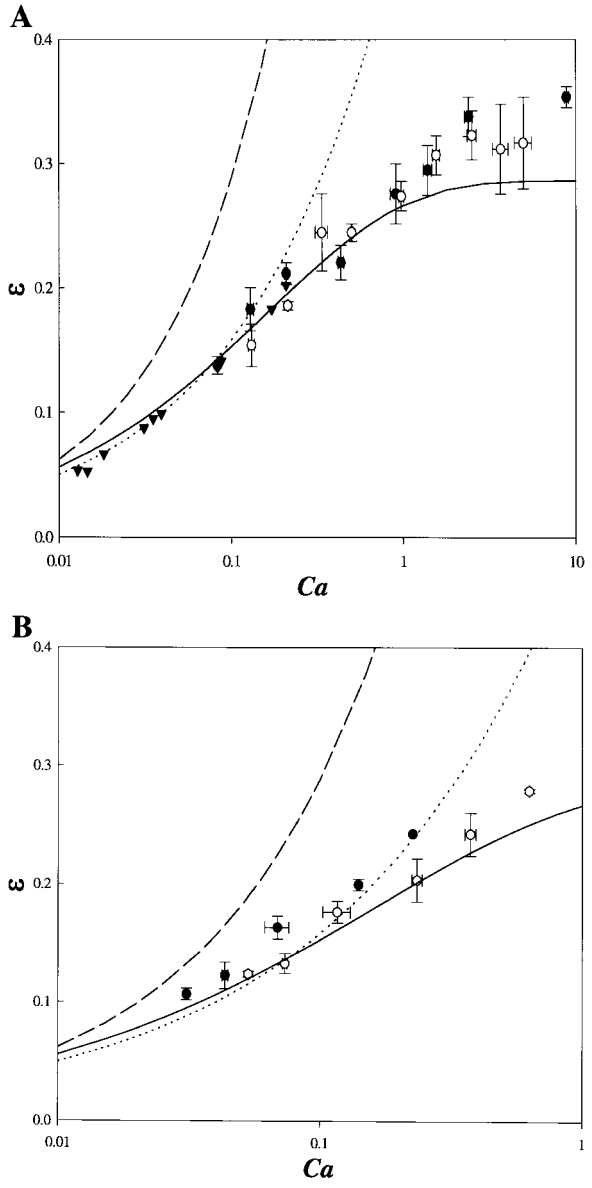

Fig. 6. $\epsilon = (a - b)/a$ vs. capillary number ($Ca = \mu_{film} U^*/\sigma^*$) of infused fluid for *systems 1* (●) and *2* (○) and Goldsmith and Mason's *system 6a* (▼; *A*) and *systems 3* (●) and *4* (○; *B*). ϵ increases with Ca, with little variation between surfactant-free and surfactant systems. See text for theoretical curves.

where $\hat{q} = -q^*\epsilon^{-3}a\mu_{film}/\sigma^*$ and $\hat{t} = t^*/(\epsilon^{-3}a\mu_{film}/\sigma^*)$. The dimensionless surface concentration $\Gamma = \Gamma^*/\Gamma^*_m = 1 + \epsilon^2\overline{\Gamma}$, where $\hat{\Gamma} = \epsilon^2\overline{\Gamma}$ and $\overline{\Gamma}$ is the variation of surface concentration from the mean. For *Eq. 3*, $|h_1| \ll 1$ and $|\hat{\Gamma}_1| \ll 1$, and substitute *Eq. 3* into *Eq. A1*. We define the dimensionless wave number $k = k^*a$ and the surface activity parameter $\hat{\delta} = \epsilon^{-2}\overline{\delta}$. The dispersion relation for $\hat{q}$ is

$$\hat{q} = \frac{k^2}{6}\left\{1 - 3\hat{\delta} - k^2 + \sqrt{\left[\left(k^2 + \frac{3}{2}\hat{\delta} - 1\right)^2 + \frac{27}{4}\hat{\delta}^2\right]}\right\} \qquad (4)$$

If $\hat{\delta} = 0$, the constant surface tension result is recovered

$$\hat{q} = \frac{k^2}{3}(1 - k^2) \qquad (5)$$

Equation 5 can also be obtained by using normal modes with Hammond's analysis (22) or in the rigid-tube limit of Halpern and Grotberg (20). In the limit $\hat{\delta} \to \infty$

$$\hat{q} = \frac{k^2}{12}(1 - k^2) \qquad (6)$$

This limit can also be obtained by applying a no-slip condition at the fluid interface. Hence, in relatively large concentrations, surfactant slows closure by up to a factor of 4. This is consistent with results of Otis et al. (35), who discussed these two limits.

THEORETICAL RESULTS

Figure 7*A* shows $\hat{q}_{max}$ vs. $\hat{\delta}$. This comes from *Eq. 4* by use of the corresponding most dangerous wave number k_{crit} at each value of $\hat{\delta}$. The $\hat{q}_{max}$ decreases with increasing surface activity. In the limit of vanishing surface activity, the growth rate approaches the constant surface tension value, $\hat{q}_{max} = 1/12$. As the interface becomes saturated with surfactant, the growth rate asymptotes to one-fourth of the surfactant-free value. This corresponds to the rigid-surface limit. Figure 7*B* shows k_{crit} vs. $\hat{\delta}$; k_{crit} varies weakly with $\hat{\delta}$. In the limit of zero surface activity, $k_{crit} = 2^{-1/2}$ is recovered. There is a minimum value of k_{crit} at $\hat{\delta} = 0.2$, and the critical wave number then asymptotes to $k_{crit} = 2^{-1/2}$ for an interface saturated with surfactant. Theoretically, typical $\overline{\delta}$ values range from 0 (no surfactant) to 8 (normal surfactant activity); $\overline{\delta} \to \infty$ represents an interface saturated with surfactant. With the assumption that $\epsilon = 0.1$–0.4, the corresponding values of $\hat{\delta}$ range up to 800 (for $0 \leq \overline{\delta} \leq 8$). In Fig. 7, for $\hat{\delta} > 1$, k_{crit} and $\hat{q}_{max}$ rapidly approach their respective asymptotic limits for an interface saturated with surfactant.

Figure 7*C* shows $\hat{q}$ vs. k for $\hat{\delta} = 0$, 0.1, 1, and ∞. The $\hat{q}_{max}$ decreases with increasing surface activity. Because the growth rate appears to be more sensitive to changes in the $\hat{\delta}$ at small values of $\hat{\delta}$, we focus on smaller values of $\hat{\delta}$ for demonstration. The k_{crit} at which the growth rate is maximum shifts slightly as $\hat{\delta}$ changes, according to Fig. 7*B*. At any given wave number, the growth rate of a disturbance is larger in a surfactant-free system than in a system with nonzero surface activity.

DISCUSSION

General observations. The growth of the disturbance is related to the ϵ in general and to the relation of ϵ to ϵ_{crit} in particular. Figure 8 shows sample data from three different experiments. We observe that for $\epsilon > \epsilon_{crit}$ (Fig. 8*A*; $\epsilon = 0.152$ compared with predicted $\epsilon_{crit} = 0.12$), the disturbance initially grows at a constant rate, which then accelerates until closure. When the disturbance amplifies, it draws fluid from the thinning region near the wall into the bulge of the film. For thin films where ϵ is just slightly larger than ϵ_{crit} (Fig. 8*B*; $\epsilon = 0.131$, predicted $\epsilon_{crit} = 0.13$), the disturbance amplifies until there is very little fluid at the wall from which to draw, so the disturbance then slows but eventually closes. For thinner films where $\epsilon < \epsilon_{crit}$ (Fig. 8*C*; $\epsilon = 0.118$, predicted $\epsilon_{crit} = 0.12$), the disturbance starts

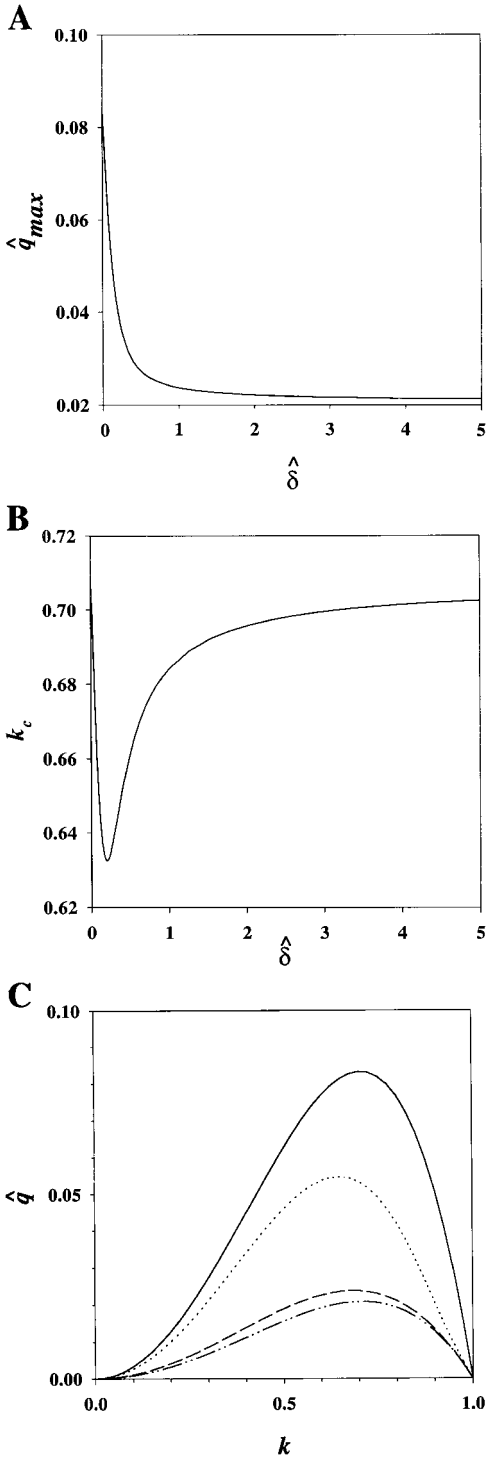

Fig. 7. Linear film stability, including surfactant effects. Maximum growth rate ($\hat{q}_{max}$) vs. surfactant activity ($\hat{\delta}$) (*A*), critical wave number (k_c) vs. $\hat{\delta}$ (*B*), and $\hat{q}$ vs. k (*C*) for (*top* to *bottom*) $\hat{\delta}$ = 0, 0.1, 1, and ∞, respectively.

with a constant growth rate followed by a slower rate, and the film never closes. We expect the disturbance amplitude to asymptote toward a constant value as $t \rightarrow \infty$, as the film forms into disconnected collars. These behavioral trends appear to be similar for all our systems, whether or not surfactant is present. We also find the region of constant growth rate to extend much further than predicted by linear theory, which assumes the growth rate constant for small h. The solid lines in Fig. 8 represent the region of constant growth; the dashed lines are an extension of the solid lines. Hence, the amplitude of the disturbance grows exponentially, even when h is not small. In Fig. 8, *A–C*, the growth

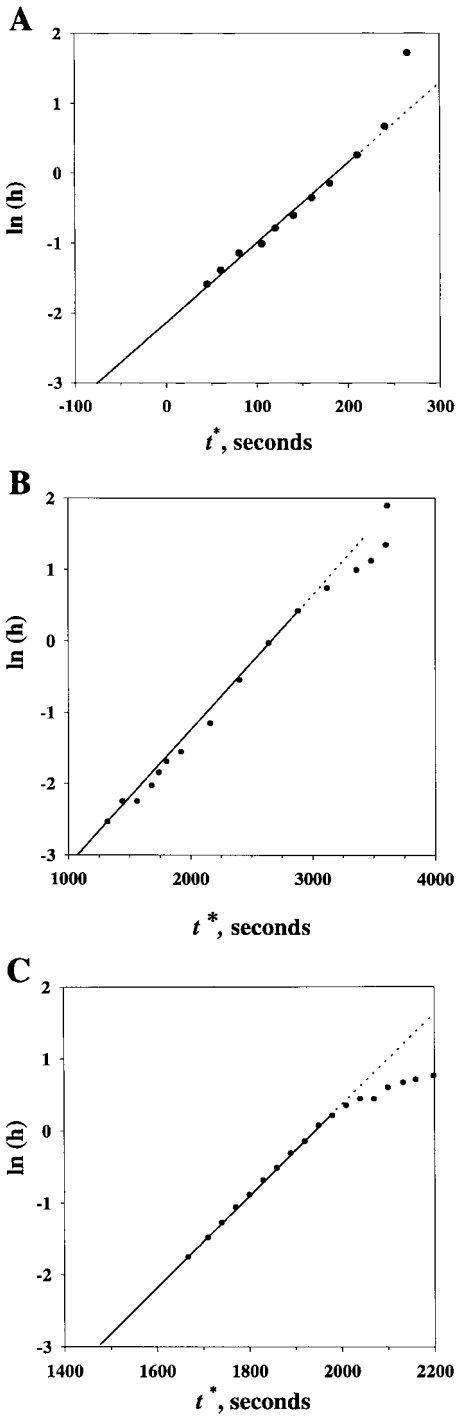

Fig. 8. Evolution of film interface vs. time; logarithm of amplitude of disturbance (h) increases with time. Disturbance initially grows at a constant rate, and then behavior depends on relationship of ϵ to ϵ_{crit}. *A: system 1*, $\epsilon = 0.152$ ($\epsilon_{crit} = 0.12$), $t_0^* \approx -76$ s, $t_f^* = 265$ s, $q^* = 0.0134$ s^{-1}. *B: system 2*, $\epsilon = 0.131$ ($\epsilon_{crit} = 0.13$), $t_0^* \approx 1{,}105$ s, $t_f^* = 3{,}610$ s, $q^* = 0.00182$ s^{-1}. *C: system 3*, $\epsilon = 0.118$ ($\epsilon_{crit} = 0.12$), $t_0^* \approx 1{,}470$ s, $q^* = 0.00641$ s^{-1}.

rate is constant until $h > 1.0$. This appears to be consistent with behavior of experiments by Goldsmith and Mason (Fig. 7 in Ref. 15). Data recorded of the small-amplitude disturbance [ln $(h) < -2.0$ in Fig. 8*B*] confirm the validity of our method determining the start time of the perturbation.

Comparison of data with theory. The experimental results support predictions that the closure time increases when surfactant is added to a system and decreases for a larger film thickness. Experimental closure times for our surfactant-free *system 1* match theory well (20) for thin films ($\epsilon < 0.20$) and are slightly underpredicted for thicker films (Fig. 4*A*). *System 2* closure times match the surfactant theory well (21) for $\epsilon < 0.20$ and are slightly overpredicted for thicker films. The addition of the surfactant PLPC to this system increases the closure time by up to a factor of 3.8 compared with the theoretical factor 4.0 for an interface saturated with surfactant (21). As ϵ increases, the discrepancy between the surfactant-free and the surfactant data is less than the theories predict. We speculate that the surfactant is less effective at delaying closure for very thick films ($\epsilon > 0.30$), when closure occurs most rapidly. For *systems 3* and *4*, the experimental closure times are underpredicted for the surfactant-free case (20) and the surfactant case (21) (Fig. 4*B*). However, the behavior of closure time decreasing with increasing film thickness appears to be accurately modeled. The addition of the surfactant Tween 20 to this system increases the closure time by up to a factor of 3.0.

The ϵ_{crit} is defined as the film thickness below which closure will not occur before infinite time. Experimentally, it is not functionally feasible to determine ϵ_{crit}. It may be more appropriate to determine a film thickness at which closure will not occur for a long time. If we define a long closure time at, e.g., $t_c = 2 \times 10^4$, then we can examine a functional ϵ_{crit} (ϵ_f) below which closure will take a long time to occur. With this in mind, we may also investigate the effect of surfactant on ϵ_f. Theory predicts that surfactant will increase ϵ_{crit} by ~10% [from $\epsilon_{crit} = 0.12$ (12) to $\epsilon_{crit} = 0.13$ (21)]. At $t_c = 2 \times 10^4$ ($t_c^* = 16$–18 min for *systems 1* and *2*) we find that ϵ_f increases >20% in the presence of PLPC, from $\epsilon_f \approx 0.13$ for *system 1* to $\epsilon_f \approx 0.16$ in *system 2*. We find that ϵ_f increases >15% in the presence of Tween 20, from $\epsilon_f \approx 0.15$ for *system 3* to $\epsilon_f \approx 0.17$ for *system 4*. Although it is possible that thinner films may be found to close at longer times, these functional values do not contradict the theory that surfactant will increase ϵ_{crit}.

Generally, our experimental results support the theoretical predictions that the growth rate decreases in the presence of surfactant and increases for thicker films. Experimental growth rates for *systems 1* and *2* are shown in Fig. 5*A*. Surfactant-free *system 1* data match Goren's theory (16) fairly well for $\epsilon < 0.2$, but q is greater than his theory for $\epsilon > 0.2$. *System 1* data are greater than our surfactant-free theory for $\epsilon < 0.2$; the theory is invalid for large ϵ. Our surfactant theory also underpredicts *system 2* data for $\epsilon < 0.2$ but accurately predicts the drop in q with the addition of surfactant. Generally, the theories underpredict the growth rates for these experiments, but our theory appears to predict a decrease in q with surfactant by an appropriate order of magnitude. We find a decrease in q from *system 1* to *system 2* to drop to as little as 21% of the surfactant-free value compared with the theoretical drop to 25% for an interface saturated with surfactant. Experimental growth rates for *systems 3* and *4* are shown in Fig. 5*B*. *System 3* data match our surfactant-free theory fairly well for $\epsilon < 0.2$. For thin films, Goren's theory overpredicts q but matches well for $\epsilon \geq 0.2$. *System 4* data fit our theory for $\epsilon \leq 0.2$, and Fig. 5*B* suggests that the surfactant activity of this Tween 20 system falls within $0.1 < \hat{\delta} < 1.0$. Our theory appears to predict q well for *systems 3* and *4* for thinner films. We find a decrease in q from *system 3* to *system 4* to drop to as little as 24% of the surfactant-free value.

Figure 6 shows how the experimental ϵ increases with Ca. Results for *systems 1* and *2* are shown in Fig. 6*A* and for *systems 3* and *4* in Fig. 6*B*. Generally, we find that the difference in film thickness formed between a surfactant-free and a surfactant system is within the experimental scatter of data. We find that the average film thickness is well predicted by the theory of Martinez and Udell (33) for *system 1* and *2* experiments, in the range $0.08 < Ca < 1$. The theory tends to underpredict ϵ as Ca reaches 10, where our experimental ϵ value approaches 0.34, vs. the calculated value of 0.295 (33). The theory of Martinez and Udell matches well and perhaps only slightly overpredicts the average ϵ values for the full range of *system 3* and *4* experiments, $0.03 < Ca < 0.63$.

Applications. Generally speaking, the airways in the lower lung of an upright human in normal gravity are those that close off first near the end of expiration. This happens because the airways are smaller in the lower regions than in the upper regions owing to the weight of the upper lung and the hydrostatic pressure gradient. In the microgravity environment, there are important changes in normal lung mechanics (36, 47) that may predispose the lung to early airway closure that is more uniformly distributed. Normally, the abdominal contents pull downward on the diaphragm in an upright human, and this tends to stretch the lung to larger volumes. Paiva et al. (36) showed that this stretching effect is lost in zero-gravity experiments, causing the lung to be smaller. Because the lung is smaller, all airway radii are also smaller and the surrounding, supportive tissue prestress is lower. This leads to a lowering of elastic recoil coupled with stronger capillary forces, since there is likely to be an increased ratio of airway liquid lining thickness to the airway radius. Both of these effects are destabilizing to the airway and could promote airway closure. Hence, in microgravity, we anticipate two important ramifications of weightlessness with regard to airway closure: *1*) airway closure could be more prevalent, and, *2*) it could occur more uniformly throughout the lung.

Airway closure may compromise gas exchange if the closing volume is too large. Also, during extravehicular activity in outer space, astronauts are protected by space suits, which have a subatmospheric internal gas

pressure requiring a larger-than-normal percentage of O_2 in the breathing gas. It is well known that a higher-than-normal percentage of O_2, if breathed long enough, will promote airway closure and collapse of alveoli (atelectasis), because portions of the lung distal to the closed airway can become "degassed" by rapid absorption of the O_2. In a setting of more uniform closure, this becomes a potentially significant issue for limited gas exchange for the astronaut. West and co-workers (19, 38, 39) measured lung function before, during (intravehicular), and after the 9-day flight of Spacelab Space Life Sciences-1. All seven crewmembers performed pulmonary function tests which showed that they experienced airway closure. Hence, gravity is not the sole contributor to airway closure phenomena that may depend more on local mechanical phenomena, as examined in the present study.

As a technologically related example, there are two air-liquid surfaces in annular extrusion methods for manufacturing small hollow fibers. An important problem in coextrusion is to have a smooth interface between the materials so that the desired mechanical and optical properties are achieved. Instabilities of this interface during concentric coextrusion are examined by Chen (3) and others.

Conclusions. Closure of the small airways of the lungs is a result of a coupled surface tension-driven and compliant wall instability. The fluid pressure drop across the air-liquid interface generated by the capillary instability drives the airway wall inward, which may induce (nonaxisymmetric) buckling and eventual collapse over the entire length of a compliant airway. In the rigid-tube model, closure cannot occur unless the film is thick enough to close, typically larger than $\epsilon = 0.12$. In a normal lung the liquid film thickness is small ($0.02 < \epsilon < 0.04$) and the tube is compliant. In a mathematical model of a liquid-lined flexible tube, Halpern and Grotberg (20) show that ϵ_{crit} is smaller for flexible tubes and decreases as the flexibility increases. Therefore, although thinner films exist in the pulmonary airways than in our present experimental model, they are still subject to a capillary-elastic instability that can lead to closure. In our model we isolate the capillary instability from the elastic and therefore must investigate films that are thick enough to close in a rigid tube. Our experiments show that surfactant has a significant effect on the growth rate and closure time of the capillary instability, and the experimental results support theory. Future experiments will examine the coupled capillary-elastic instability.

APPENDIX

Governing equations for the airway closure model with surfactant. A linear stability analysis is performed on the airway closure model with surfactant. The model is based on the analysis developed by Halpern and Grotberg (21). We use a normal-mode analysis, where $\hat{q} = \epsilon^{-3} q^*(a\mu_{film}/\sigma^*)$ is the rate of growth or decay, $\bar{\delta}$ is a surface activity parameter, and ϵ is the dimensionless unperturbed film thickness. The dimensionless surface tension is defined as $\sigma = \sigma^*/\sigma^*_m = (1 + \epsilon^2\overline{\sigma})$.

The evolution equations for the perturbation to the film thickness $[h(z, \hat{t})]$ and the surface concentration of surfactant $[\Gamma(z, \hat{t})]$ are derived from conservation of fluid mass and surfactant, based on a lubrication theory model of Halpern and Grotberg (21), and are given by

$$h_{\hat{t}} + \frac{F_z}{1 + \epsilon(h-1)} = 0, \quad F = \frac{1}{3}(1-h)^3 p_z - \frac{1}{2}(1-h)^2\,\overline{\sigma}_z$$
$$\Gamma_{\hat{t}} + f_z = 0, \quad f = \left[\frac{1}{2}(1-h)^2 p_z - (1-h)\overline{\sigma}_z\right]\Gamma \tag{A1}$$

where F is the flux of fluid, f the flux of surfactant, p is the fluid pressure, z is the axial coordinate, and $\overline{\sigma}$ is the variation of surface tension from the mean, which we assume to be small. The jump in pressure across the air-liquid interface, nondimensionalized with respect to ($\epsilon\sigma^*/a$), is proportional to the curvature of the interface and is given by $p = h_{zz} + h(1-\epsilon)^{-1}[1 + \epsilon(h-1)]^{-1}$. A linear equation of state, relating the surface tension to the surfactant concentration is used: $\overline{\sigma} = -\hat{\delta}\hat{\Gamma}$, where $\hat{\Gamma} = \Gamma - 1$ and $\hat{\delta} = \bar{\delta}/\epsilon^2$. The first terms in the expressions for the fluxes in *Eq. A1* represent capillarity effects, which are destabilizing; the second terms are stabilizing and represent the variation in surface tension gradients due to the presence of surfactant.

To compute the closure time, *Eq. A1* is solved numerically using the method of lines subject to an initially small sinusoidal disturbance with the most dangerous wavelength $\lambda = 2^{3/2}\pi$ on the basis of linear stability theory. With time, the air-liquid interface deforms and a bulge develops. For certain system parameter values, the minimum core radius, $r_{min} = 1 + \epsilon(h_{min} - 1)$, approaches a constant, and a liquid bridge does not form; for others, r_{min} starts to decrease very rapidly once it reaches a value approximately equal to 40% of the tube radius. The closure time is then taken to be the value once r_{min} reaches 0.4.

We thank Gene Kwon and Ateet Shah for efforts in obtaining the experimental data and Dr. Peter Howell, Dr. Sarah Waters, and Joseph Bull. This research was funded by National Aeronautics and Space Administration Grants NAG3-1636 and NAG-1959, National Heart, Lung, and Blood Institute Grant HL-41126, and National Science Foundation Grant CSF-9412523.

Present address of B. G. Ressler: Dept. of Biomedical Engineering, Massachusetts Institute of Technology, Cambridge, MA 02139.

Address for reprint requests and other correspondence: J. B. Grotberg, Dept. of Biomedical Engineering, University of Michigan, 3304 G. G. Brown Bldg., 2350 Hayward St., Ann Arbor, MI 48109-2125 (E-mail: grotberg@umich.edu).

Received 20 January 1998; accepted in final form 8 March 1999.

REFERENCES

1. **Agrawal, M. L., and R. D. Neuman.** Surface diffusion in monomolecular films. II. Experiment and theory. *J. Colloid Interface Sci.* 121: 366–379, 1988.
2. **Bretherton, F. P.** The motion of long bubbles in tubes. *J. Fluid Mech.* 10: 166–188, 1961.
3. **Chen, K.** Interfacial instability due to elastic stratification in concentric co-extrusion of two viscoelastic fluids. *J. Non-Newtonian Fluid Mech.* 40: 155–175, 1991.
4. **Codd, S. L., R. K. Lambert, M. R. Alley, and R. J. Pack.** Tensile stiffness of bovine tracheal wall. *J. Appl. Physiol.* 76: 2627–2635, 1994.
5. **Cox, B. G.** On driving a viscous fluid out of a tube. *J. Fluid Mech.* 14: 81–96, 1962.
6. **Crawford, A. B. H., D. J. Cotton, M. Paiva, and L. A. Engel.** Effect of airway closure on ventilation distribution. *J. Appl. Physiol.* 66: 2511–2515, 1989.

7. **Enhorning, G., L. C. Duffy, and R. C. Welliver.** Pulmonary surfactant maintains patency of conducting airways in the rat. *Am. J. Respir. Crit. Care Med.* 151: 554–556, 1995.
8. **Enhorning, G., A. Yarussi, P. Rao, and I. Vargas.** Increased airway resistance due to surfactant dysfunction can be alleviated with aerosol surfactant. *Can. J. Physiol. Pharmacol.* 74: 687–691, 1996.
9. **Everett, D. H., and J. M. Haynes.** Model studies of capillary condensation. 1. Cylindrical pore model with zero contact angle. *J. Colloid Interface Sci.* 38: 125–137, 1972.
10. **Fairbrother, F., and A. E. Stubbs.** Studies in electro-endosmosis. VI. The "bubble-tube" method of measurement. *J. Chem. Soc.* 527–529, 1935.
11. **Farstad, T., and D. Bratlid.** Pulmonary effects after surfactant treatment in premature infants with severe respiratory distress syndrome. *Biol. Neonate* 68: 246–253, 1995.
12. **Gauglitz, P. A., and C. J. Radke.** An extended evolution equation for liquid film breakup in cylindrical capillaries. *Chem. Eng. Sci.* 43: 1457–1465, 1988.
13. **Gaver, D. P., D. M. Halpern, O. E. Jensen, and J. B. Grotberg.** The steady motion of a semi-infinite bubble through a flexible-walled channel. *J. Fluid Mech.* 319: 25–65, 1996.
14. **Goerke, J., and J. A. Clements.** Alveolar surface tension and lung surfactant. In: *Handbook of Physiology. The Respiratory System. Mechanics of Breathing.* Bethesda, MD: Am. Physiol. Soc., 1986, sect. 3, vol. III, chapt. 16, p. 247–262.
15. **Goldsmith, H. L., and S. G. Mason.** The flow of suspensions through tubes. II. Single large bubbles. *J. Colloid Sci.* 18: 237–261, 1963.
16. **Goren, S. L.** The instability of an annular thread of fluid. *J. Fluid Mech.* 12: 309–319, 1962.
17. **Greaves, I. A., J. Hildebrandt, and J. F. G. Hoppin.** Micromechanics of the lung. In: *Handbook of Physiology. The Respiratory System. Mechanics of Breathing.* Bethesda, MD: Am. Physiol. Soc., 1986, sect. 3, vol. III, chapt. 14, p. 207–232.
18. **Green, F. H., S. Schurch, G. T. De Sanctis, J. A. Wallace, S. Cheng, and M. Prior.** Effects of hydrogen sulfide exposure on surface properties of lung surfactant. *J. Appl. Physiol.* 70: 1943–1949, 1991.
19. **Guy, H. J. B., G. K. Prisk, A. R. Elliott, R. A. Deutschman III, and J. B. West.** Inhomogeneity of pulmonary ventilation during sustained microgravity as determined by single-breath washouts. *J. Appl. Physiol.* 76: 1719–1729, 1994.
20. **Halpern, D., and J. B. Grotberg.** Fluid-elastic instabilities of liquid-lined flexible tubes. *J. Fluid Mech.* 244: 615–632, 1992.
21. **Halpern, D., and J. B. Grotberg.** Surfactant effects on fluid-elastic instabilities of liquid-lined flexible tubes: a model of airway closure. *J. Biomech. Eng.* 115: 271–277, 1993.
22. **Hammond, P. S.** Nonlinear adjustment of a thin annular film of viscous fluid surrounding a thread of another within a circular pipe. *J. Fluid Mech.* 137: 363–384, 1983.
23. **Howell, P., K. Cassidy, N. Gavriely, M. Glucksberg, and J. B. Grotberg.** Airway reopening: theoretical and experimental studies. *FASEB J.* 10: 4656, 1996.
24. **Im Hof, V., P. Gehr, V. Gerber, M. M. Lee, and S. Schurch.** In vivo determination of surface tension in the horse trachea and in vitro model studies. *Respir. Physiol.* 109: 81–93, 1997.
25. **Jensen, O. E., and J. B. Grotberg.** Insoluble surfactant spreading on a thin viscous film: shock evolution and film rupture. *J. Fluid Mech.* 240: 259–288, 1992.
26. **Jensen, O. E., and J. B. Grotberg.** The spreading of heat or soluble surfactant on a thin liquid film. *Phys. Fluids A* 5: 58–68, 1993.
27. **Johnson, M., R. D. Kamm, L. W. Ho, A. Shapiro, and T. J. Pedley.** The nonlinear growth of surface-tension-driven instabilities of a thin annular film. *J. Fluid Mech.* 233: 141–156, 1991.
28. **Kamm, R. D., and R. C. Schroter.** Is airway closure caused by a thin liquid instability? *Respir. Physiol.* 75: 141–156, 1989.
29. **Lee, M. M., S. Schurch, S. H. Roth, X. Jiang, S. Cheng, S. Bjarnason, and F. H. Green.** Effects of acid aerosol exposure on the surface properties of airway mucus. *Exp. Lung Res.* 21: 835–851, 1995.
30. **Liechty, E. A., E. Donovan, D. Purohit, J. Gilhooly, B. Feldman, A. Noguchi, S. E. Denson, S. S. Sehgal, I. Gross, D. Stevens, et al.** Reduction of neonatal mortality after multiple doses of bovine surfactant in low-birth-weight neonates with respiratory distress syndrome. *Pediatrics* 88: 19–28, 1991.
31. **Liu, M., L. Wang, E. Li, and G. Enhorning.** Pulmonary surfactant will secure free airflow through a narrow tube. *J. Appl. Physiol.* 71: 742–748, 1991.
32. **Macklem, P. T., D. F. Proctor, and J. C. Hogg.** The stability of peripheral airways. *Respir. Physiol.* 8: 191–203, 1970.
33. **Martinez, M. J., and K. S. Udell.** Boundary integral analysis of the creeping flow of long bubbles in capillaries. *J. Appl. Mech.* 56: 211–217, 1989.
34. **Naureckas, E. T., C. A. Dawson, B. S. Gerber, D. P. Gaver, H. L. Gerber, J. H. Linehan, J. Solway, and R. W. Samsel.** Airway reopening pressure in isolated rat lungs. *J. Appl. Physiol.* 76: 1372–1377, 1994.
35. **Otis, D. R., Jr., M. Johnson, T. J. Pedley, and R. D. Kamm.** Role of pulmonary surfactant in airway closure: a computational study. *J. Appl. Physiol.* 75: 1323–1333, 1993.
36. **Paiva, M., M. Estenne, and L. A. Engel.** Lung volumes, chest wall configuration and pattern of breathing in microgravity. *J. Appl. Physiol.* 67: 1542–1550, 1989.
37. **Plateau, J. A. F.** In: *Statique experimentale et theorique des liquides soumis aux seules forces moleculaires.* Paris: Gauthier-Villars, 1873, p. 231.
38. **Prisk, G. K., H. J. B. Guy, A. R. Elliott, R. A. Deutschman III, and J. B. West.** Pulmonary diffusing capacity, capillary blood volume, and cardiac output during sustained microgravity. *J. Appl. Physiol.* 75: 15–26, 1993.
39. **Prisk, G. K., H. J. B. Guy, A. R. Elliott, and J. B. West.** Inhomogeneity of pulmonary perfusion during sustained microgravity on SLS-1. *J. Appl. Physiol.* 76: 1730–1738, 1994.
40. **Rayleigh, L.** On the instability of a cylinder of viscous liquid under capillary force. *Phil. Mag.* 34: 145, 1892.
41. **Rayleigh, L.** On the instability of cylindrical fluid surfaces. *Phil. Mag.* 34: 177–180, 1892.
42. **Sackner, M. A., and C. S. Kim.** Phasic flow mechanisms of mucus clearance. *Eur. J. Respir. Dis. Suppl.* 153: 159–164, 1987.
43. **Schurch, S., H. Bachofen, J. Goerke, and F. Possmayer.** A captive bubble method reproduces the in situ behavior of lung surfactant monolayers. *J. Appl. Physiol.* 67: 2389–2396, 1989.
44. **Speer, C. P., O. Gefeller, P. Groneck, E. Laufkotter, C. Roll, L. Hanssler, K. Harms, E. Herting, H. Boenisch, J. Windeler, et al.** Randomised clinical trial of two treatment regimens of natural surfactant preparations in neonatal respiratory distress syndrome. *Arch. Dis. Child. Fetal Neonatal Ed.* 72: F8–F13, 1995.
45. **Taylor, G. I.** Deposition of a viscous fluid on the wall of a tube. *J. Fluid Mech.* 10: 161–165, 1961.
46. **Weibel, E. R.** *Morphometry of the Human Lung.* New York: Academic, 1963.
47. **West, J. B.** Microgravity and the lung. *Proc 12th Ann. Meeting Int. Union Physiol. Sci. Commission Gravitational Physiol., Leningrad, USSR, 1990.*
48. **Yager, D., T. Cloutier, H. Feldman, J. Bastacky, J. M. Drazen, and R. D. Kamm.** Airway surface liquid thickness as a function of lung volume in small airways of the guinea pig. *J. Appl. Physiol.* 77: 2333–2340, 1994.